An integrated simulator towards a digital twin for MW-class Gyrotrons for fusion reactors

Fusion Engineering and Design 218 (2025) 115157

Contents lists available at ScienceDirect

Fusion Engineering and Design

journal homepage: www.elsevier.com/locate/fusengdes

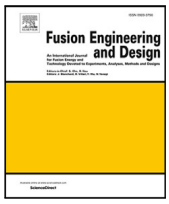

An integrated simulator towards a digital twin for MW-class Gyrotrons for fusion reactors

Elia Novarese [a], Antonio Cammi [b,c], Rosa Difonzo [a], Carolina Introini [c], Laura Savoldi [a,*]

[a] MAHTEP Group, Dipartimento Energia, Politecnico di Torino, 10124, Torino, Italy
[b] Emirates Nuclear Technology Center (ENTC), Department of Mechanical and Nuclear Engineering, Khalifa University, Abu Dhabi, 127788, United Arab Emirates
[c] Department of Energy - Nuclear Engineering Division CESNEF, Politecnico di Milano, Milano, 20133, Italy

ARTICLE INFO

Keywords:
Fusion technology
Plasma heating & current drive
Gyrotron
Digital twin
Multi-physics

ABSTRACT

In magnetic-confinement fusion reactor technology, gyrotrons are foreseen to deliver power to the plasma through mm-microwaves at a pre-determined frequency within the range of $80 - 200\ GHz$ and power of $1 - 2\ MW$. Today, only specific models focusing on specific components or specific physics of the gyrotron are available, but an overall simulator is missing. The development of a comprehensive simulator capable of describing the entire gyrotron behaviour, including its inherent nonlinearities, is crucial for accurate simulations, sensitivity analyses, operational optimization, and control purposes and represents an essential part for the definition of a new digital twin. The gyrotron is a complex device governed by multi-physics phenomena, thus the development of a simulator capable to simulate its complex dynamics requires the knowledge of the fundamental physics that describes the behaviour of all components. The goal is to develop a complete simulator of gyrotron, based on a fixed geometry and materials already selected, describing the components as objects which elaborate parameter inputs to get outputs. It is shown that in this way, the components can be seen as different boxes, the interconnections of which allow to build the simulator for the entire device. By adopting a state–space formulation, the interconnection between input and output of different blocks can be effectively managed, and through system linearization, an efficient stability analysis can be performed. In this work, each component is presented, together with its physics. The input and output parameters are then identified in order to understand how they influence the coupling between the component models and their connection. This procedure will help to build in future works the simulator of the gyrotron, aiming at developing a digital twin for it. The latter, articulated from the aggregation of simpler component models, could become a useful tool to perform complex simulations, stability analysis, optimization and control.

1. Introduction

Electron cyclotron resonance heating (ECRH) and electron cyclotron current drive (ECCD) are well-established technologies relevant to the development and operation of magnetically confined nuclear fusion reactors [1]. While the first one provides external heating to pre-heat the plasma during fusion reactor start-up, the second one provides non-inductive current drive in the plasma for steady-state operation of the reactor [1,2]. For these two technologies, the gyrotron (Fig. 1) is the power supply capable of generating high-power, high-frequency electromagnetic waves by exploiting the electron cyclotron maser instability [3].

At present, the Wendelstein 7-X (W7-X) stellarator uses 10 gyrotrons, each with an output power of 600 kW to 1 MW at a frequency of 140 GHz, and it is planned to update the fleet to 12 gyrotrons, at the same time increasing their output power in several evolutionary steps from 1 MW to 2 MW [4]. As far as future fusion reactor projects are concerned, the ECRH system for ITER foresees the implementation of 24 Gyrotrons operating at 170 GHz, each delivering 1 MW of power [5], while the EU-DEMO project foresees the installation of 32 units with the same characteristics [6]. In this context, improvements to the gyrotron performance such as the capability of operating at different frequencies [7] or strategies to improve efficiency [8] are being studied.

The modelling part is of great importance for the improvement and development of the gyrotron devices. The design of new devices from one side, as well as the control, the optimization or the analysis of the working configuration of gyrotrons already in operation on the other

* Corresponding author.
E-mail addresses: elia.novarese@polito.it (E. Novarese), antonio.cammi@ku.ac.ae (A. Cammi), rosa.difonzo@polito.it (R. Difonzo), carolina.introini@polimi.it (C. Introini), laura.savoldi@polito.it (L. Savoldi).

https://doi.org/10.1016/j.fusengdes.2025.115157
Received 17 January 2025; Received in revised form 2 May 2025; Accepted 3 May 2025
Available online 24 May 2025

Nomenclature

$\boldsymbol{B}$	Magnetic field
$\boldsymbol{E}$	Electric field
$\boldsymbol{u}$	Input vector
$\boldsymbol{v}_e$	Electron velocity
$\boldsymbol{x}$	State vector
$\boldsymbol{y}$	Output vector
I	Coil current
P	Power
p	Pressure
T	Temperature
V	Voltage
Γ	Mass rate
ρ_e	Electron density
σ	Stress profile
ϵ	Strain deformation
IN	Input variable
OUT	Output variable
abs	Absorbed
$cool$	Coolant
i	ith component
p	Parasitic
$refl$	Reflected
B.T.	Beam Tunnel
C.V.D.W.	Chemical Vapour Deposition diamond Window
CW	Continuous Wave
ECCD	Electron Cyclotron Current Drive
ECRH	Electron Cyclotron Resonance Heating
MIG	Magnetron Injection Gun
Q.O.	Quasi Optical
SC	Superconductor
TE	Transverse Electric
W7-X	Wendelstein 7-X

side, is heavily based on models. Many tools have been developed to simulate the various phenomena that occur in a gyrotron [9–11], which are essential first for the design and, in a second stage, for the analysis, control and operational enhancement of the different components of the gyrotron, and the research community is working hard to develop more sophisticated models capable of reproducing physics more accurately. In this perspective, the available models focus on specific components of the gyrotron or specific physics. For example, among others EGUN [12] is developed for particle tracking applied to the electron beam, while ARIADNE [13] and ESRAY [14] are codes for electron gun and beam tunnel simulation. EURIDICE [15] or SELFT [16] are developed to simulate the interaction behaviour between the electron beam and the electromagnetic field in the cavity, and the MUCCA tool [17] examines the multi-physics of the cavity, integrating electromagnetism, thermo-hydraulics and thermo-mechanics. So far, however, no research was specifically directed toward the development of a complete gyrotron simulator. This is a challenging problem because such a simulator must integrate multi-physics phenomena that occur on different time scales in different components with several feedback loops among the components. At the same time, only a full system simulator would allow to account for and simulate coupled effects that would not have been possible to investigate holistically before. In addition, such a gyrotron simulator would enable time-dependent simulations of the entire device, which is useful both for performing a rigorous energetic analysis and for identifying the critical points or

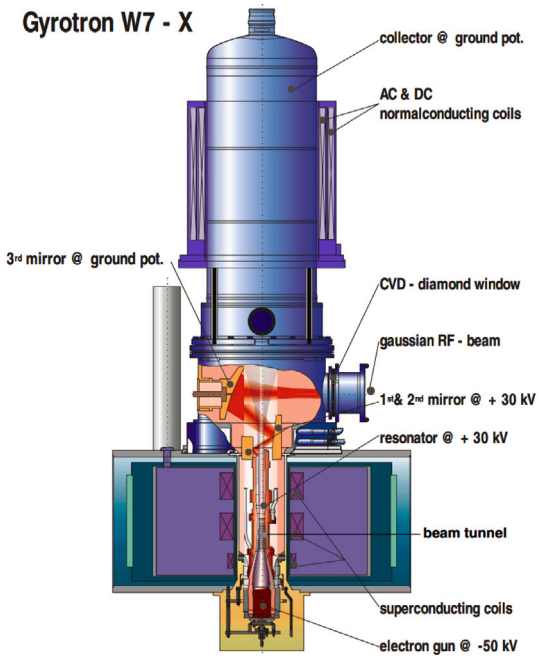

Fig. 1. Schematic view of the 140 GHz, 1 MW, CW Thales gyrotron with superconducting magnet (SCM) used in the ECH system of the W7-X stellarator [1]. CVD stands for Chemical Vapour Deposition and refers to the window.

phenomena that need to be refined, either for the control or for the management of the device during its operation. With an ability to simulate normal and off-normal working conditions, the simulator could help identifying either new or critical operating situations. However, a high-fidelity model of the entire gyrotron, if based on the available softwares and models for its components, would be computationally very demanding, and preclude real time simulations. The central aim of this work is to establish the foundation for a system simulator by characterizing each significant component of the gyrotron system. The approach creates a modular simulator architecture where individual component models connect through well-defined input/output interfaces. The state–space formulation provides a powerful mathematical framework that maintains physical accuracy while enabling computationally efficient analysis of the entire system's behaviour under various operating conditions. The benefits of developing this type of simulator are numerous: it allows understanding the impact on the whole device of replacing a component with an optimized one, or analysing the behaviour under various operational scenarios. Beyond this, it would be possible to predict new operating conditions starting from different inputs, or viceversa, as well as to determine the correct input when some constraints are applied to the operating conditions. For these reasons, an integrated simulator of the gyrotron can become essential for the development, testing, and control of this type of device. In this context, the work discussed in this article concentrates on selecting the main components of the gyrotron system, identifying their physics, and determining how they interconnect. The physics models for each component establish an input/output scheme that enables component interconnection through variable transfer among the models. The detailed phenomena occurring inside each component and the energy balance, both at component level and for the entire system, are clarified to ensure physical consistency of the simulator. While the design of each component, which is outside the scope of this work as it depends on the specs and constraints of the gyrotron in terms of frequency, power, mode of operation for which it has been designed, would require starting the discussion from the model describing the resonance cavity; here we follow a topological approach describing the gyrotron components from the bottom in, referring to

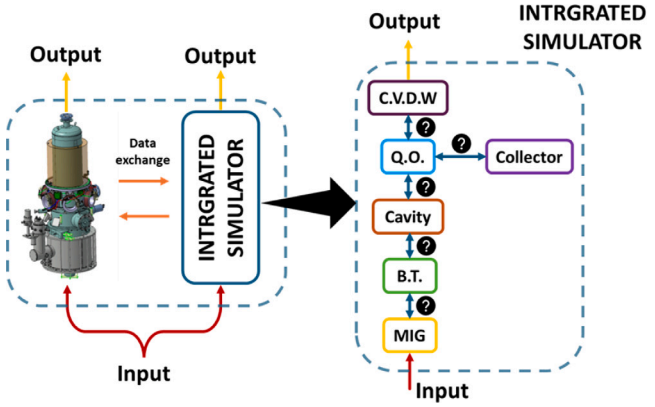

Fig. 2. The idea of having an integrated modular simulator that can reproduce the behaviour of the physical device under different operating conditions by aggregating the individual component models.

Fig. 1. Looking ahead, the gyrotron simulator developed through this approach is designed to serve as the foundation for a future digital twin application [18]. A digital twin represents a virtual replica of a physical device that maintains a bi-directional data connection with its physical counterpart, integrating physics-based simulators with real-time data from sensors, historical performance data, and machine learning algorithms (Fig. 2). This would enable real-time monitoring, predictive maintenance, operational improvement, and efficient control strategies. However, establishing the complete gyrotron simulator is the critical first step and the primary objective of the present work. The article is organized as follows: Section 2 explains the main characteristics of the system simulator to be developed for the gyrotron; in Section 3 the various selected components of the gyrotron are presented, with their phenomenology and model scheme, providing the input, output and state vector for the state space representation of each of them. In Section 4 the main concepts for the development of the gyrotron simulator are summarized, also suggesting the outlook of the next work aimed at the control phase applied to the gyrotron.

2. Strategy to develop the gyrotron simulator

The development of a digital twin is highly dependent on the integrated simulator [19]. A reliable physics-based model is essential for the control and prediction phases of a gyrotron during its operational phase, but on the other hand, computational costs counterbalance the decision to adopt high-fidelity models, requiring a trade-off between accuracy and computational time. Furthermore, the physical implementation in the model depends on what is being simulated about the device. For the control of the gyrotron, it is essential to have information about the output frequency and power, together with the efficiency of the whole device and each individual component. Information on the purity of the output mode and the level of stray radiation is also essential to determine the efficiency of the gyrotron.

From this objective, the first task is to select the components to be modelled in order to understand the main purpose that each component fulfils for the proper operation of the physical device. In this way, the simulator is built starting from the coupling of the models of the different components, each capable of simulating the main physics embedded in it. After modelling, the experimental part will be important to validate the individual model of each component and calibrate it with the experiments.

The idea behind the component model is to simulate the time evolution of the state of the component. In this way, it is possible to describe the component as a dynamic system which, given input parameters, can calculate the evolution of the state and obtain the output parameters relevant to the other component models. Thus, the model of each component is described by a system of Ordinary Differential Equations that catch the fundamental dynamics:

$$\begin{cases} \frac{d\boldsymbol{x}}{dt} = \boldsymbol{f}(\boldsymbol{x}, \boldsymbol{u}, t) \\ \boldsymbol{x}(t=0) = \boldsymbol{x}_0 \\ \boldsymbol{y} = \boldsymbol{h}(\boldsymbol{x}, \boldsymbol{u}) \end{cases} \tag{1}$$

In (1), the vector function $\boldsymbol{f} : \mathbb{R}^+ \times \mathbb{R}^n \times \mathbb{R}^m \rightarrow \mathbb{R}^n$ describes the dynamic evolution of the state vector $\boldsymbol{x} \in \mathbb{R}^n$ in the time $t \in \mathbb{R}^+$ knowing the initial state vector $\boldsymbol{x}_0 \in \mathbb{R}^n$ and the input vector parameters $\boldsymbol{u}(t) \in \mathbb{R}^m$. From the state vector solution of the model $\boldsymbol{x}(t)$, it is possible to elaborate the input vector parameters, getting the output vector $\boldsymbol{y}(t) \in \mathbb{R}^p$ which is function of the state and input vector $\boldsymbol{h} : \mathbb{R}^n \times \mathbb{R}^m \rightarrow \mathbb{R}^p$. Once the model of each component has the dynamic description of its physical behaviour, it will be possible to bring the models together to form the complete device simulator, capable of simulating the behaviour of the whole gyrotron. The idea is therefore to treat the model of each component as an object, linked to the others by parameter exchange, as schematized in Fig. 3.

In order to understand the role of each component, it is essential to understand how a gyrotron works. To generate the high-frequency, high-power electromagnetic waves, the gyrotron exploits the interaction of a helical electron beam with electromagnetic fields [20,21]. Starting from a topological description of the gyrotron behaviour, based on Fig. 1, a Magnetron Injection Gun (MIG) [22] generates the electron beam whose shape is modelled by interaction with an electric and magnetic field. The electron beam passes through a Beam Tunnel (B.T.) [23] whose main function is to suppress parasitic waves that can affect the cavity efficiency and performance due to modification of the electron beam. The electron beam, with the desired geometric and kinematic parameters, then enters the cavity [20,21]. There, the magnetic field confines the electron beam to a cyclotron frequency and its interaction with the electromagnetic field generates the Transverse Electric (TE) mode of the cavity at the chosen frequency. The electromagnetic wave beam, together with the spent electron beam, passes through a Quasi-Optical (Q.O.) system consisting of a launcher and a set of mirrors [24]. The phase correction and focusing of the wave beam occurring in that component transforms the cavity mode into a linearly polarized Gaussian wave, which is transmitted outside the gyrotron passing through a Chemical-Vapour-Deposition diamond Window (C.V.D.W.) [25]. The spent electron beam is injected into a depressed collector where part of its kinetic energy is recovered to increase the gyrotron efficiency before it strikes the collector inner wall and is absorbed. [26].

The following components must therefore be integrated and modelled in the simulator (Fig. 2):

- Magnetron Injection Gun (MIG):
- Beam Tunnel (B.T.);
- Cavity;
- Quasi-Optical (Q.O.) system;
- Chemical-Vapour-Deposition diamond Window (C.V.D.W.);
- Depressed Collector.

3. Gyrotron component and model schemes

For each of the selected components, the main functionality and phenomenology is explained in more detail and the model is presented. In each model, the links between the different physics are schematized as an exchange of input/output parameters by arrows pointing inwards (input parameters) or outwards (output parameters) from each labelled box representing a specific physics.

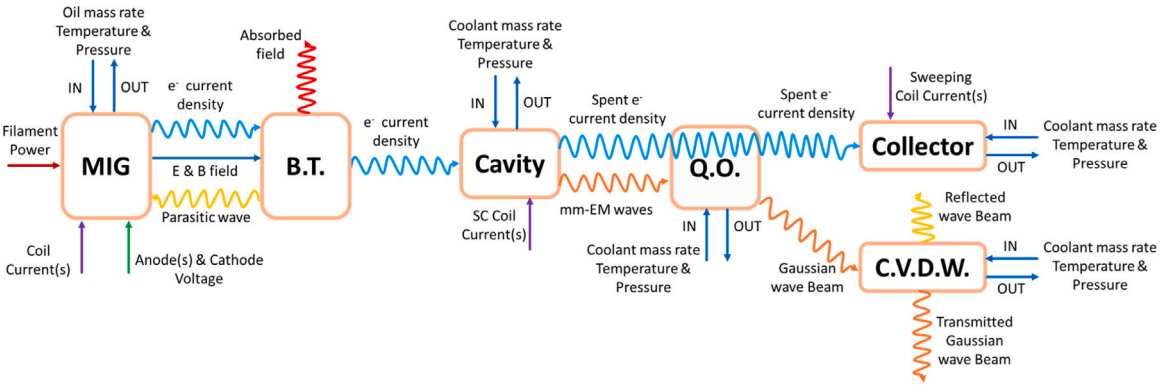

Fig. 3. The integrated simulator for the digital twin of gyrotron is built from the models of the different components. Once the input/output parameters and the dynamics of each component have been defined, it is possible to link the component models together to obtain the simulator of the gyrotron. The spent electron beam passes through the Quasi-Optical (Q.O.) system and should not touch the launcher wall. For the components in figure MIG refers to Magnetron Injection Gun, B.T. refers to Beam Tunnel, Q.O. is for Quasi-Optical system while C.V.D.W. refers to Chemical Vapour Deposition diamond Window.

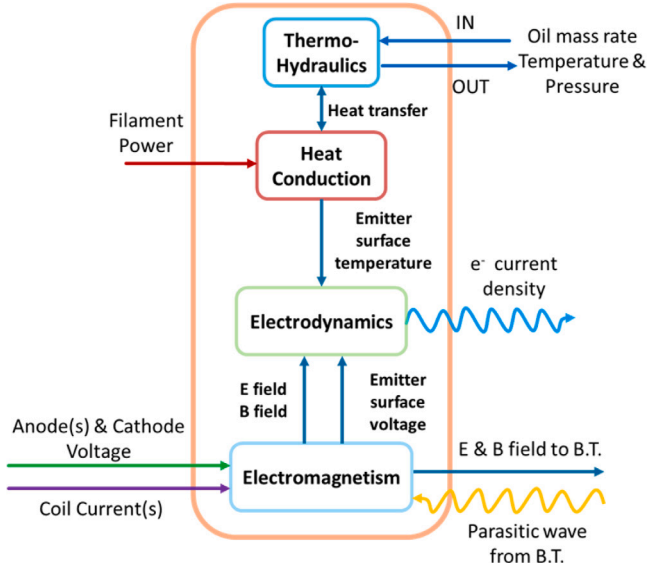

Fig. 4. The MIG model is relevant for calculating the current density from the surface of an emitter, taking into account the temperature distribution in the component and the influence of the electric and magnetic field imposed.

3.1. Magnetron injection gun

3.1.1. Phenomenology

The MIG is responsible for generating the annular electron beam [22] essential for generating the electromagnetic waves in the cavity. In this component, a tungsten emitter absorbs the radiant energy emitted by filaments, through which an electric current is passed. By absorbing energy, the emitter is heated and electrons are ejected from its surface by the thermo-ionic effect, so the emitter temperature and the voltage on the emitter surface affect the electron density current. The emitter is cooled by two main effects: the first is the expulsion of electrons from its surface as the expelled electrons have a certain amount of energy that is taken away from the emitter. The second is the diffusion of heat from the emitter to the other components of the MIG by conduction and radiation effects or convective heat transfer to the cooling oil [27].

With regard to the MIG cavity region, an electric and magnetic field are imposed to shape the generated electron beam. There are two types of MIG, depending on the type implemented in the actual gyrotrons: the diode type or the triode type. In the diode type MIG, to generate the electric field, a potential difference[1] is imposed between the cathode (the emitter) and the anode (the tube body) [28]. In the triode type, a modulation anode is added to adjust the quality of the electron beam during operation. The magnetic field is generated by a system of coils by applying an electric current to them.

3.1.2. Model

Concerning the phenomenology, in the MIG model (Fig. 4) it is important to include the thermal conduction equation. Starting from the power input to the filament component, which is a function of the electric current and the potential difference applied to it, it is possible to calculate the temperature distribution of each component incorporated in the MIG, in particular the emitter, taking into account the heat transfer by radiative effect or by contact to other components [29]. From the knowledge of the emitter temperature and its surface voltage, generated by the application of a potential difference between the cathode and the anode(s), it is possible to calculate the electron current density extracted from the emitter. The trajectory of the electrons is then influenced by the electric and magnetic field imposed to obtain the correct kinematic and geometric parameters for the electron beam to enter the cavity. Another factor affecting the electron trajectories can come from the parasitic waves that are not suppressed by the beam tunnel and propagate back to the MIG. The thermal-hydraulic model must also be used to take into account the heat transfer to the cooling oil.

The vector of input parameters for the MIG is identified by the power supplied to the filament by imposing an electric current and an electric potential difference across the filaments, the anode and cathode voltages, the parasitic waves coming from the beam tunnel and the coolant properties. The system dynamics can then be used to calculate the temperature of the various components of the MIG, which represents the state of the system, including the surface of the voltage emitter to derive the electron density current.

The corresponding input, state, and output vectors are shown in (2):

[1] With respect to the potential of the collector, which is grounded.

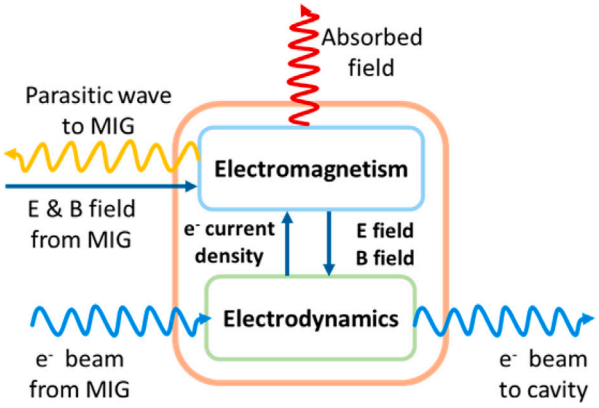

Fig. 5. The model of the beam tunnel requires the calculation of the behaviour of the parasitic waves absorbed by the inner wall of the device, as well as the influence of the electric and magnetic field on the electron beam and possible escaping waves to the MIG.

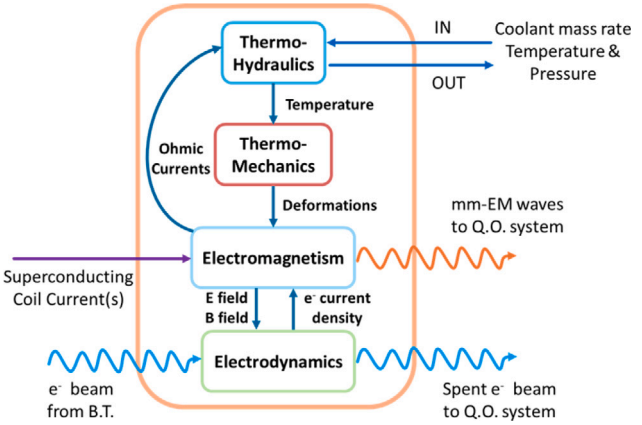

Fig. 6. The cavity model must calculate the cavity mode generated by the interaction of the electron beam and the electromagnetic field. In addition, deformations induced by the temperature distributions are relevant to account for the wave frequency shift and the stresses in the cavity structure.

$$\boldsymbol{u}_{MIG} = \begin{bmatrix} I_{filament} \\ \Delta V_{filament} \\ V_{cathode} \\ V_{anode(s)} \\ \boldsymbol{E}_p \\ \boldsymbol{B}_p \\ \Gamma_{oil}^{IN} \\ T_{oil}^{IN} \\ p_{oil}^{IN} \end{bmatrix}, \quad \boldsymbol{x}_{MIG} = \begin{bmatrix} T_i \\ \rho_e \\ \boldsymbol{v}_e \\ \boldsymbol{E} \\ \boldsymbol{B} \\ \Gamma_{oil} \\ T_{oil} \\ p_{oil} \end{bmatrix}, \quad \boldsymbol{y}_{MIG} = \begin{bmatrix} \rho_e \\ \boldsymbol{v}_e \\ \boldsymbol{E} \\ \boldsymbol{B} \\ \Gamma_{oil} \\ T_{oil} \\ p_{oil} \end{bmatrix} \tag{2}$$

where $I_{filament}$ and $\Delta V_{filament}$ are the current and potential difference applied to the filament, $V_{cathode}$ is the cathode voltage while $V_{anode(s)}$ is the anode voltage(s) (depending on the type of MIG implemented in the gyrotron being modelled). $\boldsymbol{E}$ and $\boldsymbol{B}$ are the electric and magnetic field and the pedex $\varepsilon p\varepsilon$ stays for the parasitic waves coming from the beam tunnel. ρ_e and $\boldsymbol{v}_e$ are the electron density and velocity respectively; Γ_{oil}, T_{oil} and p_{oil} are the mass rate, temperature and pressure oil respectively, T_i is the temperature of the ith component of the MIG. The superscript "IN" refers to input variables of each model.

The thermodynamics of the MIG is well described in [27,29], where a lumped model has already been shown to be sufficiently accurate to describe its phenomenology. While numerical codes such as ARIADNE [13] and ESRAY [14] are widely used for the calculation of electron trajectories.

3.2. Beam tunnel

3.2.1. Phenomenology

After leaving the MIG, the electron beam passes through the beam tunnel, an essential component in suppressing back propagation of unwanted electromagnetic waves (parasitic waves) to the MIG and deviation of the electron beam from the desired configuration. These two phenomena are closely correlated, as the parasitic waves are generated by electron beam instabilities and amplify these instabilities [30].

The beam tunnel is a waveguide whose internal structure consists of alternating rings of copper and ceramic material. The latter is a high-loss material, relevant for the absorption of parasitic waves [31]. The suppression of parasitic waves is of great importance in order to avoid the deviation of the electron beam from the correct parameters, which are essential for the desired operating condition of the cavity, and which are caused by a large energy or velocity spread of the electron beam.

For this component, it is therefore relevant to calculate the absorption efficiency of the parasitic waves and their possible leakage to the MIG, using a model capable of describing the electromagnetic interaction with the electron beam.

3.2.2. Model

The relevant task for the beam tunnel model (Fig. 5) is the computation of the parasitic waves excited by the electron beam instabilities and the feedback of these waves on the kinematic and geometrical parameters of the electron beam. This is essential to determine the state of the electron beam at the entrance of the cavity. In addition, the main objective of the beam tunnel is to suppress the parasitic waves, in order to reduce the coupling effect with the electron beam, and to prevent their back propagation to the MIG. Therefore, an important result that the beam tunnel model has to deal with is the calculation of the electromagnetic field absorbed by the beam tunnel walls and the parasitic waves that escape from it and reach the MIG. The input, state and output vectors are listed in (3):

$$\boldsymbol{u}_{BT} = \begin{bmatrix} \rho_e^{IN} \\ \boldsymbol{v}_e^{IN} \\ \boldsymbol{E}^{IN} \\ \boldsymbol{B}_{IN} \end{bmatrix}, \quad \boldsymbol{x}_{BT} = \begin{bmatrix} \rho_e \\ \boldsymbol{v}_e \\ \boldsymbol{E} \\ \boldsymbol{B} \end{bmatrix}, \quad \boldsymbol{y}_{BT} = \begin{bmatrix} \rho_e \\ \boldsymbol{v}_e \\ P_{abs} \\ \boldsymbol{E} \\ \boldsymbol{B} \end{bmatrix} \tag{3}$$

where ρ_e and $\boldsymbol{v}_e$ are the electron density and velocity respectively. $\boldsymbol{E}$ and $\boldsymbol{B}$ are the electric and magnetic fields,while $\boldsymbol{E}^{IN}$ and $\boldsymbol{B}^{IN}$ are the electric and magnetic field computed through the MIG model. P_{abs} is the absorbed power of the field and depends on the state and input vectors $P_{abs} = P_{abs}(\boldsymbol{x}_{BT}, \boldsymbol{u}_{BT})$.

Currently, the simulation tools available for the study of excited parasitic waves have been developed assuming certain approximations, e.g. NESTOR [32] assumes a constant magnetic field and radius.

3.3. Cavity

3.3.1. Phenomenology

The cavity component is a three section structure: an input downtaper and a uniform middle section followed by an output uptaper. The downtaper is required to suppress waves with frequencies below the cutoff and to reflect back waves generated in the resonant part, the resonant part being the zone where the electron generates the electromagnetic field, and the uptaper is the connecting part between the cavity and the quasi-optical system.

Electrons leaving the beam tunnel enter the downtaper as an annular beam following helical trajectories. In the resonant cavity, they interact with an almost uniform axial magnetic field generated by a superconducting coil that imposes the desired electron cyclotron frequency. With the correct parameters of the beam radius and the ratio of the transverse to the axial velocity of the electrons (α), it is possible to excite the desired cavity TE mode of the electromagnetic field at the correct frequency, and thus transfer an amount of energy to the field, generating the mm-waves [33]. In addition, the electron beam is affected by the generated electromagnetic field, so that some of the energy extracted from the wave is returned to the electron beam. This effect is relevant because, in the cavity, a net transfer of energy from the electron beam to the electromagnetic field is required for proper operation. If the cavity is not optimized in terms of efficiency, defined as the energy transferred from the electrons to the field, it is not possible to obtain high energy electromagnetic waves. This is the reason for the bunching phase phenomena between the electrons and the field [20,21]: it ensures that the majority of the electrons are gathered in the zone of the TE field where there is the possibility of transferring energy to the field [34]. In addition, if the electron beam parameters are not the nominal ones, unwanted modes will be generated on top of those expected from the cavity design, and mode competition may also occur, affecting the efficiency of the gyrotron [35]. Moreover, in the uptaper following the cavity the static and dynamic After Cavity Interaction (ACI) can rise, affecting the performance of the gyrotron [36,37]. In parallel, the generated electromagnetic waves induce relevant ohmic currents in the copper cavity wall. These parasitic currents generate a heat load profile and deformations in the cavity wall due to the temperature rise, affecting the frequency of the electromagnetic waves. This latter phenomenon is called frequency shift and its effect is of extreme importance in gyrotron operation. Therefore, an efficient cooling strategy must be adopted to limit the maximum temperature and strain in the component to avoid failure and to control the wave frequency [38].

3.3.2. Model

The cavity model (Fig. 6) must be able to simulate the waves generated, the losses on the cavity wall and their deformations. In the model, therefore, the dynamics of the electron influenced by the self-generated electromagnetic waves is relevant and is modelled by coupling an electrodynamic and an electromagnetic model, as the EURIDICE [15], SELFT [16] or TWANG [39] codes are able to reproduce. The thermo-mechanical and thermal-hydraulic models must also be taken into account, as they are essential for estimating the temperature, strain, stress profiles and possible failure of the cavity structure. In this sense, the MUCCA tool [17] has been developed to study the multi-physics phenomena arising from the cavity wall deformations induced by the ohmic currents generated by the electromagnetic field. Thus, the input parameters for the cavity model are the electron beam, the current of the superconducting coil(s) and the properties of the coolant. The input, state and output vectors for the cavity model are shown in (4):

$$\boldsymbol{u}_{cavity} = \begin{bmatrix} \rho_e^{IN} \\ \boldsymbol{v}_e^{IN} \\ I_{SC} \\ \Gamma_{cool}^{IN} \\ T_{cool}^{IN} \\ p_{cool}^{IN} \end{bmatrix}, \quad \boldsymbol{x}_{cavity} = \begin{bmatrix} \rho_e \\ \boldsymbol{v}_e \\ \boldsymbol{E} \\ \boldsymbol{B} \\ T \\ \varepsilon \\ \Gamma_{cool} \\ T_{cool} \\ p_{cool} \end{bmatrix}, \quad \boldsymbol{y}_{cavity} = \begin{bmatrix} \rho_e \\ \boldsymbol{v}_e \\ \boldsymbol{E} \\ \boldsymbol{B} \\ T \\ \sigma \\ \Gamma_{cool} \\ T_{cool} \\ p_{cool} \end{bmatrix} \tag{4}$$

where I_{SC} is the superconductor coil current(s), T is the cavity temperature profile and ε is the structure strain deformation, while σ is the stress field of the structure. The stress field is a function of the state as indicated in the output vector $\sigma = \sigma(\boldsymbol{x}_{cavity}, \boldsymbol{u}_{cavity})$.

3.4. Quasi optical system

3.4.1. Phenomenology

The wave and the electron beam then pass through the so-called Quasi Optical (Q.O.) system, which is relevant to convert the TE mode of the cavity into the mode for transmission line to the fusion reactor [40]. The Q.O. system consists of the so-called launcher and three mirrors [41]. The launcher is an oversized waveguide that has a dual function: it separates the wave beam from the electron beam, the latter passes through the system without any particular effect on the field, and it also changes the phase of the electromagnetic wave [42,43]. The aim of this correction is to transform the cavity wave mode into a linearly polarized Gaussian wave beam, which is the compatible mode of the transmission line connecting the gyrotron to the fusion reactor. The phase correction of the waves is possible thanks to perturbations of the inner wall of the launcher [44,45]. On the other hand, the three-mirror system receives the wave from the launcher to focus it using two focusing mirrors and to adjust its Gaussian wave content using a phase correction mirror, since the conversion efficiency of the launcher is limited [46]. In the inner wall of the launcher and on the surfaces of the mirrors, the incident wave induces ohmic currents, as in the cavity wall. This leads to temperature distributions in these components and the need to dissipate heat to mitigate deformations and high stresses in the structures to avoid failure. For this reason, each component of the Q.O. system also incorporates a cooling system to dissipate the induced heat. Another factor affecting the efficiency and operation of the gyrotron is the level of stray radiation that can build up in the Q.O. system [47,48].

3.4.2. Model

In summary, the model for the Q.O. system (Fig. 7) must integrate an electromagnetism model to derive the field on the surface of interest of the launcher and mirrors. The heat load is then calculated as it is important for the thermo-mechanical and thermal-hydraulic models. From these two models, the temperature, stress and strain profiles of the components are estimated, which are essential for assessing component failure and overall system efficiency. In this way, the electromagnetic waves and coolant properties are the inputs to the launcher and mirror models, which are able to calculate the efficiency of the conversion to Gaussian waves and thus estimate the wave losses, the level of stray radiation, the temperature and deformations of the structure. As for the electron beam, it passes through the launcher and the mirror towards the collector.

For the Q.O. system model, the relevant variables for the input, state and output vectors are reported in (5):

$$\boldsymbol{u}_{QO} = \begin{bmatrix} \boldsymbol{E}^{IN} \\ \boldsymbol{B}^{IN} \\ \rho_e^{IN} \\ \boldsymbol{v}_e^{IN} \\ \Gamma_{cool}^{IN} \\ T_{cool}^{IN} \\ p_{cool}^{IN} \end{bmatrix}, \quad \boldsymbol{x}_{QO} = \begin{bmatrix} \boldsymbol{E} \\ \boldsymbol{B} \\ \rho_e \\ \boldsymbol{v}_e \\ T \\ \varepsilon \\ \Gamma_{cool} \\ T_{cool} \\ p_{cool} \end{bmatrix}, \quad \boldsymbol{y}_{QO} = \begin{bmatrix} \boldsymbol{E} \\ \boldsymbol{B} \\ \rho_e \\ \boldsymbol{v}_e \\ \eta_{stray} \\ T \\ \sigma \\ \Gamma_{cool} \\ T_{cool} \\ p_{cool} \end{bmatrix} \tag{5}$$

where $\boldsymbol{E}$ and $\boldsymbol{B}$ are the wave electric and magnetic fields, T is the temperature, while ε and $\sigma = \sigma(\boldsymbol{x}_{QO}, \boldsymbol{u}_{QO})$ are the structure deformation and the stress field of the launcher or mirrors. $\eta_{stray} = \eta_{stray}(\boldsymbol{x}_{QO}, \boldsymbol{u}_{QO})$ is a factor determining the level of the stray radiation trapped.

To study the electromagnetic behaviour in the quasi-optical system, TWLDO [49] or LOT [50] are used by scholars to synthesize the quasi-optical system, while SURF3D [50] or KarLESS [51] are customarily used for the final analysis.

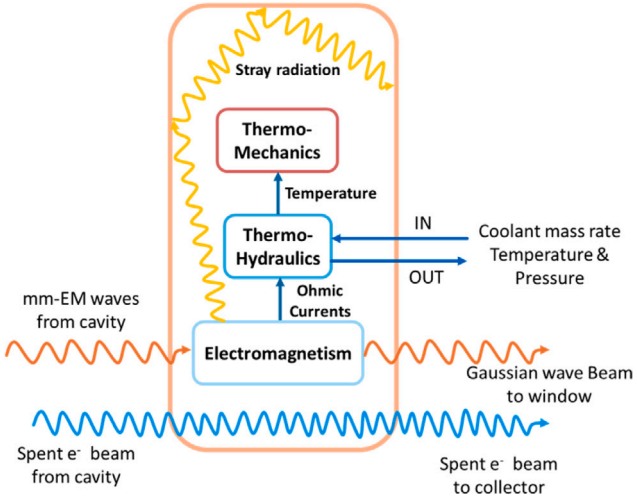

Fig. 7. In the Q.O. system model, it is relevant to calculate the transformation of the cavity mode into the Gaussian wave beam, but also the thermal load induced by the incident wave in the inner launcher wall and mirror surfaces. The stray radiation generated and trapped is also a relevant parameter for information on the efficiency of the gyrotron.

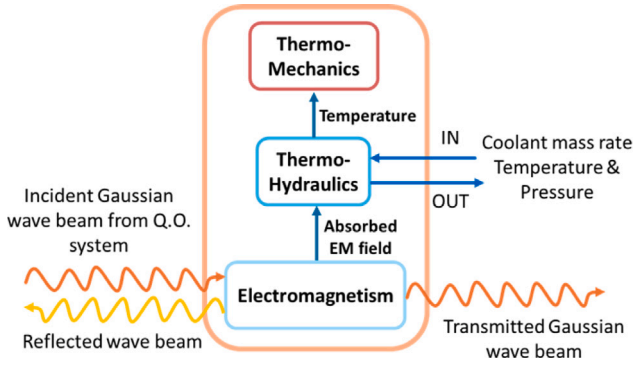

Fig. 8. In the window model, it is important to correctly calculate the energy absorbed during wave transmission through the component. This energy must be dissipated using a cooling strategy to limit window deformation and temperature. In addition, the reflected and transmitted waves are relevant to the efficiency of the gyrotron.

3.5. Window

3.5.1. Phenomenology

After passing through the Q.O. system, the electromagnetic waves are converged on the window disc. This component is responsible for isolating the internal conditions of the gyrotron from the external environment and for transmitting the received waves from the Q.O. system to the transmission line [52]. The performance of the window is therefore highly dependent on the materials used in its manufacture. In fact, it has to withstand a high static load, due to the pressure difference between the external and internal environments of the gyrotron, as its internal components operate under vacuum conditions. The window parameters related to the transmission efficiency, such as loss factor, dielectric parameters, permittivity and thickness, are very important as they affect the absorption and back reflection of the incident wave. The thickness of the window disc is designed to transmit the desired waves at a given frequency while minimizing their reflection, so that the window acts as a band-pass filter. In addition, during the wave transmission a certain amount of energy is deposited in the disc, which acts as a thermal load inducing thermal stresses. As a consequence, the window must be cooled, in order to dissipate the absorbed power and also to limit both the peak temperature and the temperature gradient according to the material properties [53].

3.5.2. Model

According to the considerations made for the window, its model (Fig. 8) must include an electromagnetism model (e.g. optical model) to describe the reflection, transmission and absorption of the incident Gaussian wave coming from the Q.O. system. From the wave absorption, it is possible to extract the thermal load in the window, which is relevant for the thermal-hydraulic and thermo-mechanical models to provide information on temperature and stress distributions. On the other hand, the transmitted wave provides the output of the complete gyrotron model in terms of power and electromagnetic wave distribution, providing information on the purity of the output mode. The model inputs are then represented by the wave coming from the Q.O. system and the coolant parameters, from which it is possible to calculate the transmission efficiency and then the thermal load and temperatures on the window structure. The input, state and output vectors for the window are listed in (6):

$$\boldsymbol{u}_{CV\,DW} = \begin{bmatrix} \boldsymbol{E}^{IN} \\ \boldsymbol{B}^{IN} \\ \Gamma_{cool}^{IN} \\ T_{cool}^{IN} \\ p_{cool}^{IN} \end{bmatrix}, \quad \boldsymbol{x}_{CV\,DW} = \begin{bmatrix} \boldsymbol{E} \\ \boldsymbol{B} \\ T \\ \sigma \\ \Gamma_{cool} \\ T_{cool} \\ p_{cool} \end{bmatrix}, \quad \boldsymbol{y}_{CV\,DW} = \begin{bmatrix} \boldsymbol{E} \\ \boldsymbol{B} \\ \boldsymbol{E}_{refl} \\ \boldsymbol{B}_{refl} \\ \varepsilon \\ \Gamma_{cool} \\ T_{cool} \\ p_{cool} \end{bmatrix} \tag{6}$$

where T is the temperature distribution of the window while σ is the stress field of the structure. The strain deformation ε is a function of the state and input vectors, $\varepsilon = \varepsilon(\boldsymbol{x}_{CV\,DW}, \boldsymbol{u}_{CV\,DW})$. $\boldsymbol{E}_{refl} = \boldsymbol{E}_{refl}(\boldsymbol{x}_{CV\,DW}, \boldsymbol{u}_{CV\,DW})$ and $\boldsymbol{B}_{refl} = \boldsymbol{B}_{refl}(\boldsymbol{x}_{CV\,DW}, \boldsymbol{u}_{CV\,DW})$ represent the reflected waves at the window.

3.6. Depressed collector

3.6.1. Phenomenology

The final component to be included in the gyrotron simulator is the depressed collector, a hollow copper cylinder responsible for absorbing the spent electrons as they leave the cavity [54]. Many collector designs have been proposed, but they all work on the same principle: as the electrons enter the collector, their trajectories are modified by a combination of magnetic and electric fields, so that the electrons are deflected towards the inner surface of the component, where they are absorbed. In the absorption region, the kinetic energy of the electrons is converted into heat, creating a corresponding thermal load profile on the inner wall [26]. If not well dissipated, these thermal loads can cause failure of the collector structure, thus compromising the operation of the gyrotron [55]. For this reason, the cooling system is also important for this type of component. In addition, collectors may use the so-called sweep coils [56], which create an alternating magnetic field that helps to spread the electrons over a larger area, thus reducing the thermal load. If a decelerating electric field is applied to the electrons, in the "depressed" collectors, part of the kinetic energy of the spent electrons is recovered, increasing the overall efficiency of the gyrotron and further reducing the thermal load on the collector wall [57].

3.6.2. Model

For the collector model (Fig. 9), the relevant task is then to calculate the heat load profile generated by the impact of the electrons on its inner wall. From this point of view, the calculation of the electron trajectories is relevant, as it is possible to extract their wall impact points, as well as their velocity and energy deposition, to obtain the

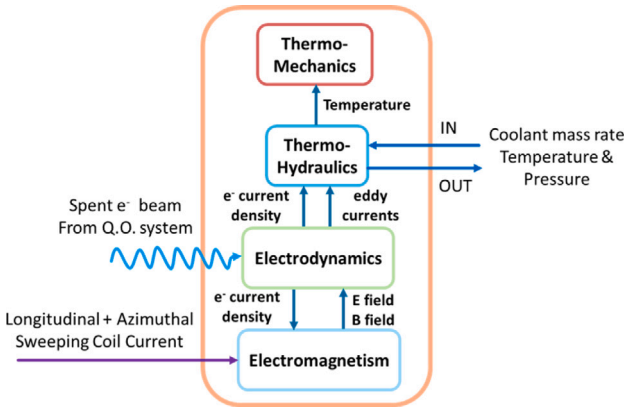

Fig. 9. The proposed model for the depressed collector must calculate the thermal load profile from the trajectories of the electrons hitting the inner wall of the collector. The thermal load profile can then be used to estimate the temperature and stresses on the structure. The electric field in the collector is generated by the potential difference between the tube body, assumed as a parameter in the model, and the collector, which is grounded [28].

heat load profile, as done in the EGUN model [12]. It is also necessary to consider the effect on the thermal load of the eddy currents induced by the alternating magnetic field of the sweep coils when they are implemented in the gyrotron. The coupling between the electrodynamic and electromagnetic models is therefore extremely important for the model in order to calculate the electron trajectories influenced by the electric and magnetic field in the collector. Once the thermal load profile has been obtained, the thermal-hydraulic and thermo-mechanical models can be used to extract the temperature and stress fields that are essential for estimating the failure and fatigue of this component. The model then receives as input the electron beam, the current of the sweep coils and the coolant properties, and from these inputs the model is able to calculate the thermal load profile, the temperature distribution and the stress profile in the structure.

The input, state and output vectors for the model of the collector are summarized in (7):

$$\boldsymbol{u}_{collector} = \begin{bmatrix} \rho_e^{IN} \\ \boldsymbol{v}_e^{IN} \\ I_{z,collector} \\ I_{\theta,collector} \\ \Gamma_{cool}^{IN} \\ T_{cool}^{IN} \\ p_{cool}^{IN} \end{bmatrix}, \quad \boldsymbol{x}_{collector} = \begin{bmatrix} \rho_e \\ \boldsymbol{v}_e \\ \boldsymbol{E} \\ \boldsymbol{B} \\ T \\ \varepsilon \\ \Gamma_{cool} \\ T_{cool} \\ p_{cool} \end{bmatrix}, \quad \boldsymbol{y}_{collector} = \begin{bmatrix} T \\ \sigma \\ \Gamma_{cool} \\ T_{cool} \\ p_{cool} \end{bmatrix} \tag{7}$$

where $I_{z,collector}$ and $I_{\theta,collector}$ are respectively the longitudinal and azimuthal sweeping coil current. ε is the strain profile in the collector structure, while σ is the stress field function of the state and input vectors, $\sigma = \sigma(\boldsymbol{x}_{collector}, \boldsymbol{u}_{collector})$.

Regarding the electron particle tracking in the collector, ARIADNE [13] and ESRAY [14] high-fidelity numerical codes widely used in the design and simulation process.

4. Conclusion and perspective

The creation of a gyrotron simulator requires as a first step the implementation of an integrated and purpose-built simulator capable of representing the key phenomena and physics occurring within its components, including the system's inherent nonlinearities, for a fixed geometry and materials already selected of the device. To address this challenge, we identified the main components present in the physical device. Regarding the integrated system simulator for the gyrotron, the relevant components have been identified, along with their interconnections, to obtain information on the power, frequency, effectiveness and output mode quality of the electromagnetic waves generated:

- the magnetron injection gun, which generates the electron current density;
- the beam tunnel, which absorbs parasitic waves and reduces electron beam instabilities;
- the cavity, which generates electromagnetic waves at the specified TE mode and frequency;
- the quasi optical system, which adapts the cavity's electromagnetic waves to match the external transmission line mode;
- the window, which transmits the waves outside the gyrotron;
- the depressed collector, which captures the spent electron beam while reclaiming part of its kinetic energy to boost the gyrotron's overall performance.

The components have been organized considering their phenomenology and multiphysics interactions. The relevant physical models of each component use state–space formulation to simplify their interconnection, through defined input and output vector parameters and state space vectors, and permit systematic stability analysis through linearization. The simulator requires several specialized models working together: an electrodynamic model for electron behaviour influenced by the gyrotron's electromagnetic fields; an electromagnetic model to calculate fields throughout the system, from cavity-generated waves to the fields shaping the electron beam; a thermodynamic model for temperature distribution in component structures, paired with a thermo-hydraulic model describing various cooling systems; and a thermo-mechanical model for components requiring strain and stress profile evaluation. After identifying, these physical models, the next step in building the gyrotron simulator will involve a preliminary modal analysis of the cavity. The state–space formulation will support stability analysis, providing insights into how cavity radius changes or electron current variations affect the system. This methodical approach will produce a simulator suitable for accurate reproduction of system behaviour, sensitivity studies, and the development of control strategies for the entire system. Looking ahead, this gyrotron simulator will serve as the foundation for a digital twin application that connects the virtual simulator with the physical device through sensor data and machine learning techniques, enabling advanced monitoring and control capabilities.

CRediT authorship contribution statement

Elia Novarese: Writing – review & editing, Writing – original draft, Supervision, Methodology, Conceptualization. **Antonio Cammi:** Writing – review & editing, Visualization, Supervision, Methodology, Conceptualization. **Rosa Difonzo:** Supervision. **Carolina Introini:** Supervision. **Laura Savoldi:** Writing – review & editing, Supervision, Methodology, Conceptualization.

Funding

This publication is part of the project PNRR-NGEU which has received funding from the MUR – DM 118/2023.

Declaration of competing interest

The authors declare the following financial interests/personal relationships which may be considered as potential competing interests: Elia Novarese reports financial support was provided by PNRR-NGEU MUR 118-2023. This publication is part of the project PNRR-NGEU which has received funding from the MUR – DM 118/2023. If there are other authors, they declare that they have no known competing financial interests or personal relationships that could have appeared to influence the work reported in this paper.

Acknowledgement

The authors would like to thank Professor Konstantinos Avramidis for his advice and invaluable help on the state of the art of the gyrotron components and models presented.

Data availability

No data was used for the research described in the article.

References

[1] M.K. Thumm, G. Denisov, K. Sakamoto, M.Q. Tran, High-power gyrotrons for electron cyclotron heating and current drive, Nucl. Fusion 59 (7) (2019) 073001, http://dx.doi.org/10.1088/1741-4326/ab2005.

[2] S. Freethy, L. Figini, S. Craig, M.A. Henderson, R. Sharma, T. Wilson, The optimisation of the step electron cyclotron current drive concept, Nucl. Fusion (2024) http://dx.doi.org/10.1088/1741-4326/ad7a8a.

[3] J. Huang, T. Song, C. Zhang, W. Wang, K. Zhang, M. Hu, Z. Wu, R. Zhong, J. Zhou, T. Zhao, et al., Theoretical investigations on forward-wave and backward-wave operation of a frequency-tunable gyrotron, IEEE Trans. Electron Devices 67 (9) (2020) 3809–3814, http://dx.doi.org/10.1109/TED.2020.3009960.

[4] H. Laqua, K. Avramidis, H. Braune, I. Chelis, G. Gantenbein, S. Illy, Z. Ioannidis, J. Jelonnek, J. Jin, L. Krier, et al., The ECRH-power upgrade at the Wendelstein 7-X stellarator, in: EPJ Web of Conferences, vol. 277, EDP Sciences, 2023, p. 04003, http://dx.doi.org/10.1051/epjconf/202327704003.

[5] M. Tran, P. Agostinetti, G. Aiello, K. Avramidis, B. Baiocchi, M. Barbisan, V. Bobkov, S. Briefi, A. Bruschi, R. Chavan, et al., Status and future development of heating and current drive for the EU DEMO, Fusion Eng. Des. 180 (2022) 113159, http://dx.doi.org/10.1016/j.fusengdes.2022.113159.

[6] G. Granucci, F. Auriemma, L. Aucone, B. Baiocchi, N. Bonanomi, F. Braghin, A. Bruschi, D. Busi, I. Casiraghi, F. Fanale, et al., Roles of ECH system in DTT plasma operations, Nucl. Fusion (2023) http://dx.doi.org/10.1088/1741-4326/ad7742.

[7] Q. Liu, Q. Zhao, Y. Zhang, X. Zeng, E. Wang, P. Pan, J. Feng, Design consideration of cavity and MIG of a 170/230-GHz dual-frequency megawatt-class gyrotron for CFETR, IEEE Trans. Plasma Sci. 51 (1) (2023) 83–89, http://dx.doi.org/10.1109/TPS.2022.3231355.

[8] B.F. Ell, C. Wu, G. Gantenbein, S. Illy, M.S. Misko, I.G. Pagonakis, J. Weggen, M. Thumm, J. Jelonnek, Toward the first continuous wave compatible multistage depressed collector design for high power gyrotrons, IEEE Trans. Electron Devices 70 (3) (2023) 1299–1305, http://dx.doi.org/10.1109/TED.2023.3234885.

[9] M. Damyanova, E. Balabanova, S. Kern, S. Illy, S. Sabchevski, M. Thumm, E. Vasileva, I. Zhelyazkov, Simulation tools for computer-aided design and numerical investigations of high-power gyrotrons, J. Phys.: Conf. Ser. 356 (1) (2012) http://dx.doi.org/10.1088/1742-6596/356/1/012044.

[10] M. Damyanova, S. Kern, S. Illy, M. Thumm, S. Sabchevski, I. Zhelyazkov, E. Vasileva, Modelling and simulation of gyrotrons for ITER, J. Phys.: Conf. Ser. 516 (1) (2014) http://dx.doi.org/10.1088/1742-6596/516/1/012028.

[11] M. Damyanova, S. Sabchevski, I. Zhelyazkov, E. Vasileva, E. Balabanova, P. Dankov, P. Malinov, Problem-oriented simulation packages and computational infrastructure for numerical studies of powerful gyrotrons, J. Phys.: Conf. Ser. 715 (1) (2016) http://dx.doi.org/10.1088/1742-6596/715/1/012001.

[12] W.B. Herrmannsfeldt, EGUN: An Electron Optics and Gun Design Program, Tech. Rep., SLAC National Accelerator Lab., Menlo Park, CA (United States), 1988, http://dx.doi.org/10.2172/6711732.

[13] J. Pagonakis, J. Vomvoridis, The self-consistent 3D trajectory electrostatic code ARIADNE for gyrotron beam tunnel simulation, in: Infrared and Millimeter Waves, Conference Digest of the 2004 Joint 29th International Conference on 2004 and 12th International Conference on Terahertz Electronics, 2004, http://dx.doi.org/10.1109/ICIMW.2004.1422262.

[14] S. Illy, Untersuchungen von Strahlinstabilitäten in der Kompressionszone von Gyrotron-Oszillatoren mit Hilfe der kinetischen Theorie und zeitabhängiger Particle-in-Cell-Simulationen (Ph.D. thesis), Universität Karlsruhe (TH), 1997, http://dx.doi.org/10.5445/IR/105397.

[15] K.A. Avramides, I.G. Pagonakis, C.T. Iatrou, J.L. Vomvoridis, EURIDICE: A code-package for gyrotron interaction simulations and cavity design, in: EPJ Web of Conferences, vol. 32, EDP Sciences, 2012, p. 04016, http://dx.doi.org/10.1051/epjconf/20123204016.

[16] S. Kern, Numerische simulation der gyrotron-wechselwirkung in koaxialen resonatoren (Ph.D. thesis, Dissertation), Karlsruhe, Karlsruher Institut für Technologie (KIT), 1996, 1996, http://dx.doi.org/10.5445/IR/55396.

[17] L. Savoldi, K.A. Avramidis, F. Albajar, S. Alberti, A. Leggieri, F. Sanchez, A validation roadmap of multi-physics simulators of the resonator of MW-class CW gyrotrons for fusion applications, Energies 14 (23) (2021) 8027, http://dx.doi.org/10.3390/en14238027.

[18] F. Tao, B. Xiao, Q. Qi, J. Cheng, P. Ji, Digital twin modeling, J. Manuf. Syst. 64 (2022) 372–389, http://dx.doi.org/10.1016/j.jmsy.2022.06.015.

[19] A. Thelen, X. Zhang, O. Fink, Y. Lu, S. Ghosh, B.D. Youn, M.D. Todd, S. Mahadevan, C. Hu, Z. Hu, A comprehensive review of digital twin—part 1: modeling and twinning enabling technologies, Struct. Multidiscip. Optim. 65 (12) (2022) 354, http://dx.doi.org/10.1007/s00158-022-03425-4.

[20] G.S. Nusinovich, Introduction to the Physics of Gyrotrons, JHU Press, 2004.

[21] M. Kartikeyan, E. Borie, M. Thumm, Gyrotrons: High-power microwave and millimeter wave technology, in: Advanced Texts in Physics, Springer, Heidelberg, 2004, http://dx.doi.org/10.1007/978-3-662-07637-8.

[22] L. Zhang, L.J. Nix, A.W. Cross, Magnetron injection gun for high-power gyroklystron, IEEE Trans. Electron Devices 67 (11) (2020) 5151–5157, http://dx.doi.org/10.1109/TED.2020.3025747.

[23] K.A. Avramidis, A. Marek, I. Chelis, Z.C. Ioannidis, L. Feuerstein, J. Jelonnek, M. Thumm, I. Tigelis, Simulation of parasitic backward-wave excitation in high-power gyrotron cavities, IEEE Trans. Electron Devices 70 (4) (2023) 1898–1905, http://dx.doi.org/10.1109/TED.2023.3242216.

[24] G. Zhao, Q. Xue, Y. Wang, X. Wang, S. Zhang, G. Liu, J. Feng, L. Zhang, Design of quasi-optical mode converter for 170-GHz TE 32, 9-mode high-power gyrotron, IEEE Trans. Plasma Sci. 47 (5) (2019) 2582–2589, http://dx.doi.org/10.1109/TPS.2019.2908503.

[25] M.K. Alaria, Y. Choyal, A. Sinha, Design of single-disk RF window for high-power gyrotron, IEEE Trans. Plasma Sci. 40 (11) (2012) 3052–3055, http://dx.doi.org/10.1109/TPS.2012.2212464.

[26] L. Savoldi, C. Bertani, F. Cau, F. Cismondi, G. Gantenbein, S. Illy, G. Monni, Y. Rozier, R. Zanino, Towards the optimization of the thermal–hydraulic performance of gyrotron collectors, Fusion Eng. Des. 100 (2015) 120–132, http://dx.doi.org/10.1016/j.fusengdes.2015.04.044.

[27] C. Introini, N. Badodi, R. Bertazzoni, G. Carannante, J.-P. Hogge, S. Illy, A. Leggieri, F. Sanchez, L. Savoldi, A. Cammi, Sensitivity analysis of the lumped thermal model of the EU 170 GHz gyrotron magnetron injection gun, IEEE Trans. Plasma Sci. (2024) http://dx.doi.org/10.1109/TPS.2023.3348171.

[28] S. Illy, S. Kern, I.G. Pagonakis, A. Vaccaro, Collector loading of the 2-MW, 170-GHz gyrotron for ITER in case of beam power modulation, IEEE Trans. Plasma Sci. 41 (10) (2013) 2742–2747, http://dx.doi.org/10.1109/TPS.2013.2262607.

[29] N. Badodi, A. Cammi, A. Leggieri, F. Sanchez, L. Savoldi, A new lumped approach for the simulation of the magnetron injection gun for megawatt-class EU gyrotrons, Energies 14 (8) (2021) 2068, http://dx.doi.org/10.3390/en14082068.

[30] M. Pedrozzi, S. Alberti, J.P. Hogge, M.Q. Tran, T.M. Tran, Electron beam instabilities in gyrotron beam tunnels, Phys. Plasmas 5 (6) (1998) 2421–2430, http://dx.doi.org/10.1063/1.872918.

[31] N. Kumar, M.K. Alaria, U. Singh, A. Bera, T.P. Singh, A.K. Sinha, Design of beam tunnel for 42 GHz, 200 kW gyrotron, J. Infrared Millim. Terahertz Waves 31 (2010) 601–607, http://dx.doi.org/10.1007/s10762-009-9614-3.

[32] I.G. Chelis, K.A. Avramidis, J.L. Vomvoridis, Resonant modes of disk-loaded cylindrical structures with open boundaries, IEEE Trans. Microw. Theory Tech. 63 (6) (2015) 1781–1790, http://dx.doi.org/10.1109/TMTT.2015.2420093.

[33] A. Fliflet, M. Read, K. Chu, R. Seeley, A self-consistent field theory for gyrotron oscillators: Application to a low Q gyromonotron, Int. J. Electron. Theor. Exp. 53 (6) (1982) 505–521, http://dx.doi.org/10.1080/00207218208901545.

[34] K.R. Chu, The electron cyclotron maser, Rev. Modern Phys. 76 (2004) 489–540, http://dx.doi.org/10.1103/RevModPhys.76.489.

[35] J. Genoud, Advanced Linear Models for Gyro-Backward Wave Instabilities in Gyrotrons (Ph.D. thesis), EPFL, 2019, http://dx.doi.org/10.5075/epfl-thesis-9503.

[36] V. Zapevalov, M. Moiseev, Influence of aftercavity interaction on gyrotron efficiency, Radiophys. Quantum Electron. 47 (7) (2004) 520–527, http://dx.doi.org/10.1023/B:RAQE.0000047243.18212.1d.

[37] K.A. Avramidis, Z.C. Ioannidis, S. Kern, A. Samartsev, I.G. Pagonakis, I.G. Tigelis, J. Jelonnek, A comparative study on the modeling of dynamic after-cavity interaction in gyrotrons, Phys. Plasmas 22 (5) (2015) 053106, http://dx.doi.org/10.1063/1.4919924.

[38] A. Bertinetti, K. Avramidis, F. Albajar, F. Cau, F. Cismondi, Y. Rozier, L. Savoldi, R. Zanino, Multi-physics analysis of a 1MW gyrotron cavity cooled by mini-channels, Fusion Eng. Des. 123 (2017) 313–316, Proceedings of the 29th Symposium on Fusion Technology (SOFT-29) Prague, Czech Republic, September 5-9, 2016, https://doi.org/10.1016/j.fusengdes.2017.05.016.

[39] S. Alberti, T. Tran, K. Avramides, F. Li, J.-P. Hogge, Gyrotron parasitic-effects studies using the time-dependent self-consistent monomode code TWANG, in: 2011 International Conference on Infrared, Millimeter, and Terahertz Waves, IEEE, 2011, pp. 1–2, http://dx.doi.org/10.1109/irmmw-THz.2011.6105097.

[40] M.K. Alaria, A. Sinha, H. Khatun, Design and development of mode launcher for high frequency gyrotron, Infrared Phys. Technol. 75 (2016) 187–192, http://dx.doi.org/10.1016/j.infrared.2015.12.011.

[41] J. Jin, B. Piosczyk, M. Thumm, T. Rzesnicki, S. Zhang, Quasi-optical mode converter/mirror system for a high-power coaxial-cavity gyrotron, IEEE Trans. Plasma Sci. 34 (4) (2006) 1508–1515, http://dx.doi.org/10.1109/TPS.2006.877627.

[42] Z. Guohui, X. Jing, G. Zhigang, Z. Heng, Y. Hongfang, Study on high power gyrotron multimode coupling launcher, AIP Adv. 13 (2) (2023) 025259, http://dx.doi.org/10.1063/5.0138774.

[43] U.U. Farid, U. Fazri, Theory and Algorithms for a Quasi-Optical Launcher Design Method for High-Frequency Gyrotrons (Ph.D. thesis), 2013.
[44] A. Bogdashov, G. Denisov, Asymptotic theory of high-efficiency converters of higher-order waveguide modes into eigenwaves of open mirror lines, Radiophys. Quantum Electron. 47 (4) (2004) 283–296, http://dx.doi.org/10.1023/B:RAQE.0000047649.17664.6e.
[45] A. Chirkov, G. Denisov, M. Kulygin, V.I. Malygin, S. Malygin, A. Pavel'ev, E. Soluyanova, Use of Huygens' principle for analysis and synthesis of the fields in oversized waveguides, Radiophys. Quantum Electron. 49 (2006) 344–353, http://dx.doi.org/10.1007/s11141-006-0067-4.
[46] J. Jin, Quasi-Optical Mode Converter for a Coaxial Cavity Gyrotron (Ph.D. thesis), Citeseer, 2007, http://dx.doi.org/10.5445/IR/270067871.
[47] M.P. Perkins, R. Cao, J.M. Neilson, R.J. Vernon, A high efficiency launcher and mirror system for use in a 110 GHz TE 22, 6 mode gyrotron, Int. J. Infrared Millim. Waves 28 (2007) 207–218, http://dx.doi.org/10.1007/s10762-007-9200-5.
[48] B. Piosczyk, O. Braz, G. Dammertz, C. Iatrou, S. Illy, M. Kuntze, G. Michel, A. Mobius, M. Thumm, V. Flyagin, V. Khishnyak, A. Pavelyev, V. Zapevalov, Coaxial cavity gyrotron with dual RF beam output, IEEE Trans. Plasma Sci. 26 (3) (1998) 393–401, http://dx.doi.org/10.1109/27.700770.
[49] J. Jin, J. Flamm, J. Jelonnek, S. Kern, I. Pagonakis, T. Rzesnicki, M. Thumm, High-efficiency quasi-optical mode converter for a 1-MW $TE_{32,9}$-mode gyrotron, IEEE Trans. Plasma Sci. 41 (10) (2013) 2748–2753, http://dx.doi.org/10.1109/TPS.2013.2261322.
[50] J. Neilson, Surf3d and LOT : computer codes for design and analysis of high-performance QO launchers in gyrotrons, 2004, pp. 667–668, http://dx.doi.org/10.1109/ICIMW.2004.1422267.
[51] A. Marek, J. Jin, J. Jelonnek, M. Thumm, A.-S. Müller, Development of an advanced vector analysis code for simulation of electromagnetic fields in quasi-optical systems of high power gyrotrons, in: 2017 Eighteenth International Vacuum Electronics Conference, IVEC, 2017, pp. 1–2, http://dx.doi.org/10.1109/IVEC.2017.8289599.
[52] M. Thumm, Development of output windows for high-power long-pulse gyrotrons and EC wave applications, Int. J. Infrared Millim. Waves 19 (1998) 3–14, http://dx.doi.org/10.1023/A:1022514528711.
[53] M.K. Alaria, Y. Choyal, A.K. Sinha, Design of single-disk RF window for high-power gyrotron, IEEE Trans. Plasma Sci. 40 (11) (2012) 3052–3055, http://dx.doi.org/10.1109/TPS.2012.2212464.
[54] V. Manuilov, M. Morozkin, O. Luksha, M.Y. Glyavin, Gyrotron collector systems: Types and capabilities, Infrared Phys. Technol. 91 (2018) 46–54, http://dx.doi.org/10.1016/j.infrared.2018.03.024.
[55] C. Baxi, R. Callis, I. Gorelov, J. Lohr, Thermal stress analysis of 1MW gyrotron collector, Fusion Eng. Des. 82 (5) (2007) 731–735, Proceedings of the 24th Symposium on Fusion Technology, https://doi.org/10.1016/j.fusengdes.2007.01.016.
[56] V. Manuilov, D. Smirnov, S. Malygin, E. Soluyanova, Numerical simulation of the gyrotron collector systems with rotating magnetic field, in: Infrared and Millimeter Waves, Conference Digest of the 2004 Joint 29th International Conference on 2004 and 12th International Conference on Terahertz Electronics, 2004, IEEE, 2004, pp. 663–664, http://dx.doi.org/10.1109/ICIMW.2004.1422265.
[57] I.G. Pagonakis, J.-P. Hogge, S. Alberti, K.A. Avramides, J.L. Vomvoridis, A new concept for the collection of an electron beam configured by an externally applied axial magnetic field, IEEE Trans. Plasma Sci. 36 (2) (2008) 469–480, http://dx.doi.org/10.1109/TPS.2008.917943.